Annals of Materials Science & Engineering

Open Access

Austin Publishing Group

Research Article

Design of Titanium Dioxide-Based Nanocomposites for Efficient Dark Photocatalytic Processes

Abdul Noman Razzaq[1]*, Abubaker Aslam[2], Abubakar Saddique[3], Farrukh Saleem Raza[4], Waseem Imtiaz[4], Muhammad Yousaf[5]

[1]School of Physics, University of Agriculture, 38000, Faisalabad, Pakistan

[2]School of Physics, Xi'an Jiaotong University, Xi'an, Shaanxi 710049, P.R. China

[3]Hangzhou Institute for Advanced Study, Hangzhou 310024; University of Chinese Academy of Sciences, China

[4]School of Material Science and Engineering, Xi'an Jiaotong University, Xi'an, Shaanxi 710049, P.R. China

[5]Department of Physics, University of Agriculture, 38000, Faisalabad. Punjab, Pakistan

***Corresponding author:** Abdul Noman Razzaq, School of Physics, University of Agriculture, Faisalabad, Pakistan

Email: raqnoman85@gmail.com

Received: November 08, 2025

Accepted: December 20, 2025

Published: December 31, 2025

Abstract

Titanium dioxide is a very important metal oxide semiconductor and has its applications in almost every sphere of life including photocatalysis because of its distinct optical nature. Its large band gap (BG) (3-3.2 eV) allows under sunlight. The main focus of this research was to increase the photocatalytic activity of TiO2 doping with metal such as silver nitrate (AgNO3). TiO2 was prepared by sol-gel method and silver nitrate was prepared by hydrothermal method. After preparation TiO2 and AgNO3 both were doped with each other. The main purpose is to study the kinetics of the dilapidation process of due and reactions by varying photocatalytic parameters under sunlight. The synthesized composite was employed as a catalyst for photocatalytic degradation of methyl blue (MB) in aqueous media. Dissimilar variations such as initial dye concentration, time exploring, loading of catalyst and pH of solution were used to check the photocatalytic activity of pure and doped TiO2. The obtained result suggested that the dye TiO2-AgNO3 composite shows the highest degradation rate at pH-11 with the optimized amount of 2mg catalyst and concentration 20ppm under sunlight. The doped TiO2-AgNO3 composite exhibit more photocatalytic performance as compared to the pure TiO2. Prepared TiO2 based composite was characterized by FTIR, XRD, and SEM/EDX. Prepared composite much better photocatalytic performance than pure TiO2 for water purification and environmental purification.

Keywords: Photocatalyst; TiO_2; $AgNO_3$; Sol–gel; Water purification; Dye degradation; Methylene Blue

Introduction

The photocatalytic activity of titanium dioxide (TiO_2) was first demonstrated by Honda and Fujishima in 1972, when they reported its ability to drive water splitting under ultraviolet (UV) irradiation [1]. Since then, TiO_2 has emerged as one of the most versatile semiconductor materials, with widespread applications in water purification, fuel cells, self-cleaning coatings, solar energy conversion, biomedical implants, and as a pigment in paints, food additives, and pharmaceuticals [2,3]. Its technological significance lies in its unique combination of chemical stability, non-toxicity, corrosion resistance, low cost, and favorable optical and electronic properties, making it a benchmark photocatalyst for environmental and energy-related applications [4].

Structurally, TiO_2 exists in three crystalline polymorphs: anatase, rutile, and brookite. Anatase and rutile, both tetragonal in structure, are the most studied due to their photocatalytic activity. Anatase possesses a band gap (Eg) of ~3.2 eV, slightly higher than that of rutile (~3.0 eV), and is generally considered the more active phase under UV irradiation [5,6]. However, mixed anatase–rutile systems often demonstrate superior photocatalytic performance due to synergistic charge separation effects [7]. Phase transformation between anatase and rutile is strongly dependent on synthesis method, particle size, and calcination temperature, typically occurring above 450–600 °C via oxygen vacancy-mediated rearrangements [8].

Despite its advantages, a major limitation of TiO_2 is its wide band gap, which restricts absorption primarily to the UV region ($\lambda < 400$ nm), accounting for less than 5% of solar radiation. To address this, various modification strategies have been investigated, including metal/non-metal doping, surface sensitization, and semiconductor coupling. Among these, doping with transition metals (e.g., Fe, Cu, Zn), noble metals (e.g., Ag, Pt), and rare-earth elements has proven particularly effective in extending TiO_2 absorption into the visible spectrum, suppressing charge recombination, and enhancing photocatalytic activity [9,10,11]. For example, Ag- and Cu-doped TiO_2 systems have demonstrated significant improvements in the degradation of organic dyes and other pollutants under solar irradiation [12].

Dye pollutants, especially methylene blue (MB), remain a major environmental challenge due to their persistence, complex aromatic structures, and resistance to conventional treatment methods. Advanced oxidation processes (AOPs) such as photocatalysis offer a sustainable solution, enabling complete mineralization of dyes under mild operating conditions [13]. Recent studies have further demonstrated that coupling TiO_2 with silver-based compounds (e.g., $AgNO_3$, Ag nanoparticles) enhances electron trapping, promotes charge separation, and increases visible light responsiveness, making such composites promising candidates for wastewater remediation [14,15].Building on this background, the present study focuses on the synthesis and photocatalytic evaluation of an $AgNO_3$–TiO_2 nanocomposite. TiO_2 nanoparticles were prepared via a sol–gel method, while $AgNO_3$ was synthesized hydrothermally and subsequently integrated to form the composite. The photocatalytic performance of the $AgNO_3$–TiO_2 system was assessed by the degradation of methylene blue under light irradiation. The findings aim to advance the development of cost-effective and visible-light-active photocatalysts for environmental remediation.

Abdul Noman Razzaq © All rights are reserved

Citation: Abdul Noman Razzaq, Abubaker Aslam, Abubakar Saddique, Farrukh Saleem Raza, Waseem Imtiaz, Muhammad Yousaf. Design of Titanium Dioxide-Based Nanocomposites for Efficient Dark Photocatalytic Processes. Ann Materials Sci Eng. 2025; 9(1): 1053.

Materials and Methods

Materials

The chemicals used in this study included hydrochloric acid (HCl), acetic acid (CH_3COOH), distilled water, ethanol (C_2H_5OH), and titanium tetra-iso-propoxide (TTIP) as the titanium precursor. Acetyl acetone was employed as a stabilizing agent, while methylene blue (MB) served as the model dye pollutant. All reagents were of analytical grade and were used without further purification.

Instruments and Equipment's:

The subsequent instrument was used in this experiment as shown in Table 1.

Preparation of Stock Solutions of Methylene Blue (MB):

Stock and working solutions of methylene blue (MB) were prepared for photocatalytic experiments. A 1000 ppm stock solution was obtained by dissolving 100 mg of MB in 100 mL of distilled water with thorough stirring. From this, a series of working solutions (5, 10, 20, 40, 60, and 100 ppm) were prepared by appropriate dilution with distilled water. The 20 ppm solution was further adjusted to different pH values to evaluate the photocatalytic activity of pure TiO_2 as shown in Figure 1.

Table 1: Equipment's list.

Sr. No.	Apparatus name	Specifications
1	Oven	Lab tech
2	Furnace	ZTML104
3	pH meter	OHAUS, STARTER300
4	Sonicator	Elamsonic
5	UV-Vis spectroscopy	190-1100
6	Autoclave reactors	Capacity of 80 ml

This table shows the list of main equipment used during the synthesis and characterization processes. Each instrument was selected based on precision and reliability for material preparation and analysis.

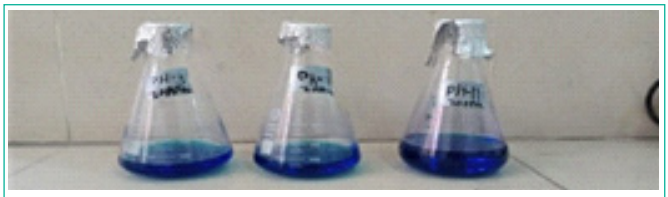

Figure 1: The image shows three conical flasks labeled with different pH values (e.g., pH-3, pH-7, pH-11) containing blue-colored solutions, likely used during the synthesis of TiO_2 nanomaterials.

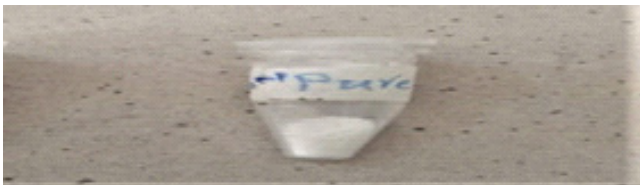

Figure 2: The image shows a small vial containing white powder, likely the TiO_2 nanoparticles obtained after the synthesis process.

Figure 3: The image shows two small vials labeled "Pure" — the left one contains a blue-colored solution, while the right one appears colorless or lighter after exposure to sunlight. This illustrates the photocatalytic performance of pure TiO_2 nanoparticles.

Among the various reported approaches for TiO_2 synthesis—such as hydrothermal, deposition, and sol–gel methods—the sol–gel technique was selected in this work due to its simplicity, cost-effectiveness, and ability to produce highly crystalline anatase-phase nanoparticles with narrow particle size distribution [16,17].

Sol–Gel Method

The sol–gel method allows for precise control over stoichiometry, phase composition, and morphology, making it highly suitable for photocatalyst preparation. Compared with the hydrothermal route, the sol–gel process produces smaller, more crystalline TiO_2 nanoparticles under identical conditions [18]. Calcination temperature strongly influences particle size, surface area, and pore structure, with higher temperatures favoring growth and partial anatase–rutile phase transition [19].

Advantages of the Sol–Gel Method:

The sol–gel process offers several advantages:

- Formation of thin and uniform films with good adhesion to substrates.
- Cost-effectiveness and scalability.
- Capability to fabricate complex geometries.
- Tunable composition and structure.
- Corrosion resistance and protective properties of derived coatings.

Experimental Procedure for TiO_2 Synthesis

TiO_2 nanoparticles were synthesized using titanium tetra-iso-propoxide (TTIP) as a precursor. First, 8.11 g of acetyl acetone was placed in a 500 mL beaker under continuous magnetic stirring. Subsequently, 22.39 g of TTIP was added dropwise to the solution while maintaining vigorous stirring. In a separate beaker, 4.82 g of acetic acid was diluted with 200 mL of distilled water.

The dilute acetic acid solution was then added dropwise (one drop every two seconds) from a burette into the TTIP–acetyl acetone mixture, which was continuously stirred. After complete addition, the mixture was stirred for an additional 1 h to obtain a homogeneous sol. The resulting sol was stored in a sealed plastic container at 4 °C until further use. volumetric ratio of precursors used as shown in Table 2.

Synthesis of TiO_2 Nanoparticles from TiO_2 Sol

Ten milliliters of the prepared TiO_2 sol were dried at 70 °C for 8 h to obtain a TiO_2 xerogel. The dried material was ground with a mortar and pestle to form a fine powder. The resulting powder was then calcined at 600 °C for 2 h in a muffle furnace to yield uniform TiO_2 nanoparticles (Figure 2).

Photocatalytic Testing of Pure TiO_2

The photocatalytic activity of the synthesized TiO_2 nanoparticles was tested using a 20 ppm MB solution. Small bottles were labeled, and each was filled with 10 mL of 20 ppm MB solution adjusted to pH 11. To each bottle, 2 mg of pure TiO_2 nanoparticles was added. The suspensions were exposed to direct sunlight, and the degradation activity was monitored (Figures 3).

Preparation of 1% Silver Nitrate ($AgNO_3$) Solution

A 1% $AgNO_3$ solution was prepared by dissolving 0.01 g of silver nitrate in 10 mL of distilled water. The solution was magnetically stirred for 2 h, then stored in a tightly sealed plastic container at 4 °C as shown in Figure 4.

Figure 4: The image shows a **magnetic stirrer with heating** — a common lab device used to mix and gently heat solutions uniformly.

Figure 5: The image shows microcentrifuge tubes containing white and off-white powder samples, labeled differently — likely representing doped TiO_2 (titanium dioxide) nanoparticles synthesized under various conditions or with different dopants.

Figure 6: The image shows two sets of bottles — one set with a blue-colored solution and the other appearing colorless or lighter after exposure, likely indicating a photocatalytic activity test of $AgNO_3$–TiO_2 nanocomposite under sunlight.

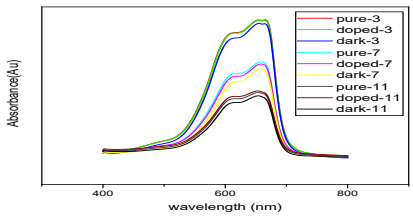

Figure 7: This image shows a UV–Visible absorption spectrum comparing pure and doped TiO_2 samples under different conditions (labeled as pure-3, doped-3, dark-3, etc.).

Hydrothermal Method (Background)

The hydrothermal technique involves crystallization of nanomaterials in aqueous solution under controlled temperature and pressure [20]. Unlike the sol–gel method, it can produce highly crystalline nanoparticles without post-calcination. Despite its advantages, the process is less controllable due to complex electrochemical and thermodynamic factors.

Preparation of $AgNO_3$–TiO_2 Nanocomposites

$AgNO_3$–TiO_2 nanocomposites were prepared by mixing TiO_2 sol with varying amounts of $AgNO_3$ solution, followed by drying and calcination. Four compositions were prepared:

- **1:10 ratio** – 1 mL $AgNO_3$ added to 10 mL TiO_2 sol, dried at 70 °C for 15 h.
- **1:20 ratio** – 0.05 mL $AgNO_3$ added to 10 mL TiO_2 sol, dried at 80 °C for 12 h.
- **1:40 ratio** – 0.25 mL $AgNO_3$ added to 10 mL TiO_2 sol, dried at 80 °C for 12 h.
- **1:120 ratio** – 0.0083 mL $AgNO_3$ added to 10 mL TiO_2 sol, dried at 80 °C for 12 h.

All dried samples were collected in glass Petri dishes (Figure 3.9), ground into fine powders, and calcined at 600 °C for 2 h **(Figure. 5).** The resulting $AgNO_3$–TiO_2 powders are shown in Figure 5.

Optimization of $AgNO_3$–TiO_2 Photocatalysts

The photocatalytic activity of $AgNO_3$–TiO_2 composites with different Ag:TiO_2 ratios (1:20, 1:30, 1:40, 1:120) was evaluated against 20 ppm MB solution at pH 11. For each test, 2 mg of catalyst was added to 10 mL of MB solution in labeled bottles. The suspensions were exposed to sunlight for 2 h, and dye degradation was monitored as shown in Figure 6. Among the tested samples, the 1:120 $AgNO_3$–TiO_2 composite showed the highest degradation efficiency

Characterization Techniques

The synthesized nanomaterials were characterized using multiple analytical techniques. Scanning electron microscopy (SEM) was employed to investigate the surface morphology and particle distribution of TiO_2 and $AgNO_3$–TiO_2 composites. Atomic force microscopy (AFM) provided high-resolution topographic images and enabled conductance measurements at the nanoscale. X-ray diffraction (XRD) analysis was carried out to confirm the crystal structure and estimate the average crystallite size of the samples. Additionally, Fourier transform infrared spectroscopy (FTIR) was used to identify surface functional groups and verify the chemical bonding within the nanomaterials.

Photocatalytic Degradation of Methylene Blue (MB)

Photocatalytic degradation experiments were carried out using both pure TiO_2 and $AgNO_3$–TiO_2 nanocomposites under sunlight. Reaction parameters were varied as follows:

- **pH effect (3, 7, 11):** Solutions adjusted with HCl or NaOH; optimum degradation was observed at pH 11.
- **Catalyst dose:** Different masses of catalyst were tested in 10 mL MB solution at pH 11 to study the influence of dosage.
- **Dye concentration:** MB solutions of 10 ppm and 20 ppm were used to study degradation efficiency.
- **Irradiation time:** Experiments were conducted for 15, 35, and 50 minutes to monitor time-dependent degradation.

UV–Vis spectrophotometry was used to record absorption spectra, and degradation efficiency was calculated using Beer–Lambert's law. Results confirmed superior photocatalytic performance of $AgNO_3$–TiO_2 composites compared to pure TiO_2.

Results and Discussion

Photodegradation Behavior of $AgNO_3$–TiO_2 Systems

Effect of pH on MB Degradation

The pH of the solution is a critical factor influencing the photocatalytic activity of TiO_2-based systems because it affects the surface charge of the catalyst, the ionization state of the dye, and the generation of reactive species. As shown in Figure 7, methylene blue

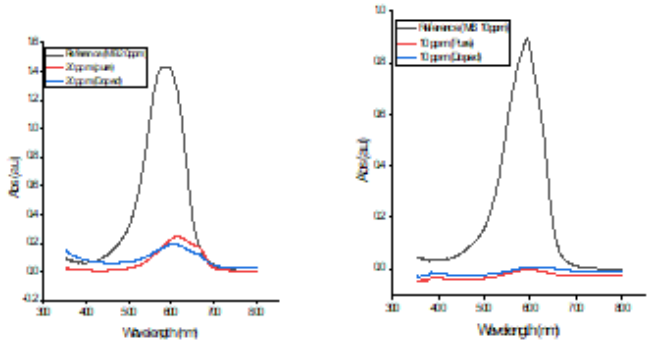

Figure 8: These two graphs show UV–Vis absorption spectra of methylene blue (MB) solutions at different concentrations (20 ppm and 10 ppm), comparing pure TiO_2 and doped TiO_2 photocatalysts.

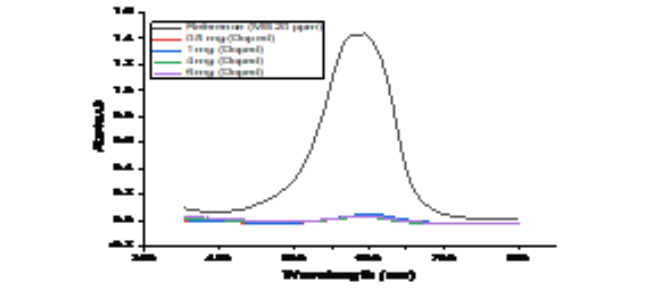

Figure 9: This graph shows the UV–Vis absorption spectra of methylene blue (MB, 20 ppm) after photocatalytic treatment using different dosages of doped TiO_2 catalyst (0.5 mg, 1 mg, 4 mg, 6 mg).

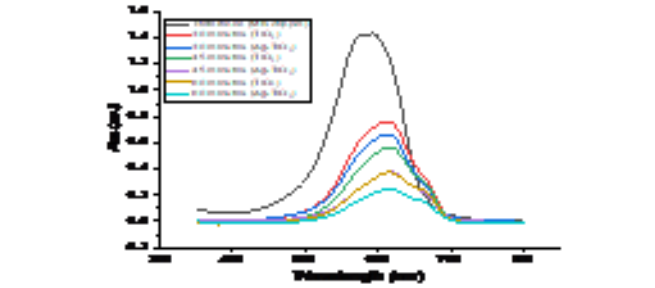

Figure 10: This graph shows UV–Vis absorption spectra of methylene blue (MB, 20 ppm) under photocatalytic degradation using TiO_2 and Ag–TiO_2 catalysts for different exposure times (30, 45, and 60 minutes).

(MB) degradation efficiency increased significantly with increasing alkalinity. At pH 11, almost 90% of MB was degraded within 80 minutes under sunlight irradiation, whereas the rates at pH 3 and 7 were considerably lower. This can be explained by the mechanism of hydroxyl radical formation. At higher pH values, hydroxide ions (OH^-) are more abundant and readily interact with photogenerated holes in TiO_2 to form hydroxyl radicals (·OH), which are strong oxidizing agents responsible for dye degradation. Conversely, under acidic conditions, the surface of TiO_2 becomes positively charged, which can repel cationic dyes such as MB and reduce adsorption efficiency. Previous studies also reported similar behavior, showing that alkaline conditions favor ·OH-mediated oxidation pathways, while acidic conditions promote hole-driven oxidation [21 Therefore, the results indicate that alkaline environments are more effective for MB photodegradation with $AgNO_3$–TiO_2, as they facilitate both dye adsorption and ·OH generation as shown in Figure 7.

Effect of Initial Dye Concentration

The degradation efficiency was also dependent on the initial MB concentration. Figure. 8 shows that the doped catalyst performed better than pure TiO_2 at both 10 ppm and 20 ppm, with the improvement being more pronounced at higher concentration. At low MB concentrations, most dye molecules are effectively degraded because sufficient active sites are available on the catalyst surface. However, at higher concentrations, competition for active sites increases, and the penetration of photons into the solution decreases due to dye shielding effects. Despite this, $AgNO_3$–TiO_2 maintained higher activity than pure TiO_2, suggesting that doping improved charge separation and extended the lifetime of reactive species. This implies that silver species play a role in trapping electrons, thereby reducing recombination and allowing more efficient utilization of photogenerated holes and radicals as shown in Figure 8.

Effect of Catalyst Dosage

The effect of catalyst dosage was examined by varying $AgNO_3$–TiO_2 amounts between 0.5 and 6 mg in 10 mL MB solution (10 ppm). Figure. 9 indicates that increasing dosage beyond a certain point did not significantly enhance degradation efficiency (Figure 9).

At lower dosages, degradation is limited by the availability of active sites. However, excessive catalyst loading leads to particle agglomeration and turbidity, which reduce the penetration of light into the suspension and increase scattering effects. This results in fewer photons reaching the catalyst surface, thereby reducing the efficiency of the photocatalytic process. Thus, there is an optimum dosage beyond which no further benefit is achieved, and in some cases, performance can even decline. This observation aligns with literature reports where excessive photocatalyst concentrations hinder reaction efficiency due to light attenuation and catalyst aggregation as shown in Figure. 9.

Effect of Irradiation Time

The impact of irradiation duration was studied at constant pH (11) and catalyst loading (2 mg). As shown in Figure.10 both pure and doped TiO_2 showed increasing MB degradation with longer irradiation times, but the doped system consistently outperformed pure TiO_2 as shown in Figure 10.

This behavior is expected, as prolonged irradiation allows more electron–hole pairs to be generated, increasing the likelihood of pollutant degradation. However, the superior performance of $AgNO_3$–TiO_2 highlights the role of silver species in suppressing recombination and facilitating electron transfer. The data indicate that doped catalysts are more efficient at sustaining photocatalytic activity over time, which is crucial for practical wastewater treatment applications.

The absorbance of the remaining dye solution was measured using a UV-Vis spectrophotometer in the 400–700 nm wavelength range. The maximum absorbance (λ_max = 484 nm) was determined, and the photodegradation of MB was measured at different time intervals. The percentage degradation of MB was calculated using the following equation [22].

$$= \frac{A_\theta - A_t}{A_\theta} \times 100$$

Anywhere A_θ is the maximum preoccupation at zero time and A_t is the maximum obsession at maximum time or when the degradation process is complete. Percentage Degradation Efficiency of Pure and Ag doped TiO_2 as shown in Table 3. Ag-TiO_2 is about 9 % more efficient than the pure.

Characterization of Catalysts

X-ray Diffraction (XRD)

XRD patterns (Figure 11) confirmed that calcined TiO_2 and $AgNO_3$–TiO_2 samples were mainly composed of anatase with traces of rutile. The anatase phase is known to exhibit superior photocatalytic

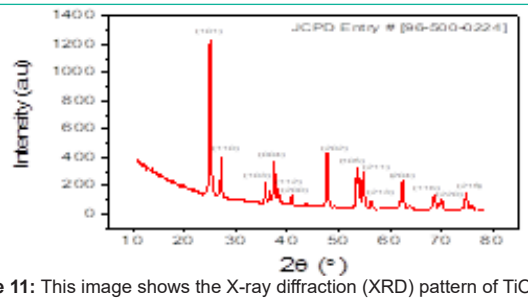

Figure 11: This image shows the X-ray diffraction (XRD) pattern of TiO_2 (titanium dioxide), a common method used to identify its crystalline phase and structure.

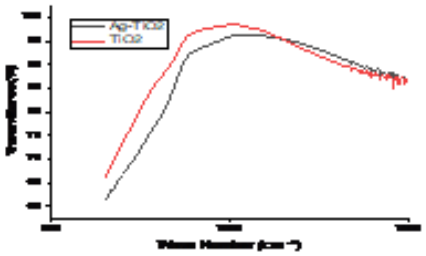

Figure 12: This image shows the FTIR (Fourier Transform Infrared) spectra of pure TiO_2 and Ag–TiO_2 nanocomposite samples. FTIR is used to identify the functional groups and chemical bonding present in the materials.

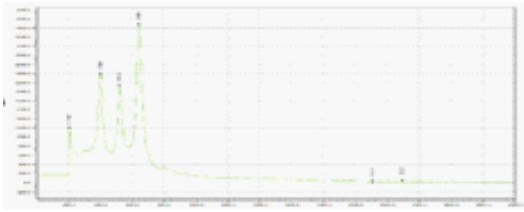

Figure 13: This image shows the Raman spectrum of Ag–TiO_2, which is used to identify the crystalline phase, structural properties, and effects of doping on TiO_2.

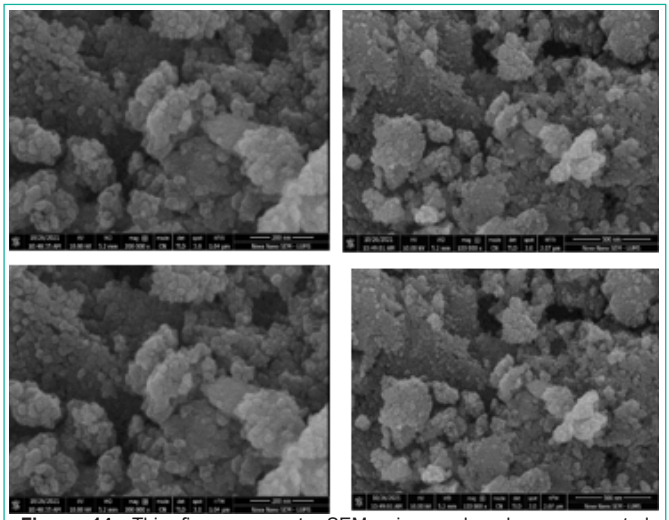

Figure 14: This figure presents SEM micrographs show aggregated nanostructures composed of uniformly distributed TiO_2 nanoparticles. The particles appear to have a spherical to slightly irregular morphology, with sizes typically in the nanometer range (20–50 nm). The agglomeration observed is due to the high surface energy and strong interparticle interactions among TiO_2 nanoparticles. The surface texture indicates a porous structure, which is beneficial for applications such as photocatalysis and adsorption.

activity compared to rutile, due to its higher surface area and lower recombination rate of charge carriers. With increasing calcination temperature (300–800 °C), diffraction peaks became sharper and more intense, indicating improved crystallinity and larger particle sizes.

The relative proportion of rutile also increased with calcination temperature, consistent with the anatase-to-rutile phase transformation. Since rutile generally shows lower photocatalytic activity, maintaining anatase-rich structures is beneficial. The incorporation of $AgNO_3$ appears to stabilize the anatase phase, thereby enhancing photocatalytic efficiency, as show in Figure 11.

Based on the observed diffraction peaks, the average particle size was estimated using the Debye–Scherrer equation, while the interplanar spacing (d-spacing) was determined using Bragg's Law. The calculated values are summarized in Table X.

$$\boldsymbol{D=(0.9\,\lambda)/\beta Cos\theta}$$

$$\boldsymbol{2dsin\theta=n\lambda}$$

Where, λ is wavelength of X-Ray (0.1540 nm), β is FWHM (full width at half maximum), θ is diffraction angle, d is d- spacing and D is particle diameter size and XRD Spectra Peak Identification and Crystallite Size calculation as shown in Table 4.

Average Crystallite Size = 26.42 nm

Mineral Type: Anatase

Crystal System: Tetragonal

Fourier Transform Infrared Spectroscopy (FTIR)

FTIR spectra **(Figure. 12)** revealed characteristic Ti–O stretching vibrations below 1000 cm^{-1}. Although no distinct silver-related peaks were observed, silver doping influenced the intensity and shape of absorption bands, suggesting interaction between silver species and the TiO_2 lattice.

Annealing reduced hydrogen-bonding features, while hydroxyl-related bands became more evident at higher calcination temperatures (≈500 °C). Hydroxyl groups on the surface are known to act as active sites for ·OH radical generation, which directly contributes to enhanced photocatalytic activity. Therefore, the presence of surface hydroxyls in the doped system may explain its improved performance compared to pure TiO_2, as shown as Figure 12.

Raman Analysis

Raman spectroscopy is a powerful technique for investigating the vibrational properties of Ag–TiO_2 nanoparticles. The recorded Raman spectra (Figure 13) confirm the successful formation of Ag-doped TiO_2, consistent with the XRD and FTIR results. Prominent Raman bands were observed at 202.4, 400.3, 540.8, and 635 cm^{-1}, which are attributed to Ti–O vibrational modes of TiO_2.

Notably, the intensity of the characteristic Raman peaks increased upon Ag loading. This enhancement can be attributed to the influence of metal doping, which is known to modify the crystal structure, particle size, morphology, and specific surface area of TiO_2. In this study, the stronger Raman signals of the Ag-doped TiO_2 nanotubes, compared to the undoped samples, indicate improved crystallinity, further confirming the structural refinement induced by silver incorporation, as shown in Figure 13.

Scanning Electron Microscopy (SEM)

SEM images (Figure.14) of pure TiO_2 revealed nanoscale particles with moderate aggregation. In the $AgNO_3$–TiO_2 system, larger clusters (~5–6 μm) were observed, within which $AgNO_3$ nanoparticles of

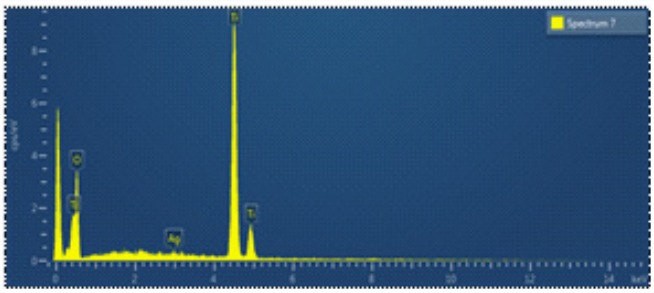

Figure 15: EDX spectrum confirms the presence of Ti, O, and Ag, indicating the formation of pure Ag–TiO_2. The Ag peak around 3 keV verifies successful silver incorporation onto the TiO_2 surface without impurities.

Table 2: volumetric ratio of precursors used.

Sample Name	TTiP	Acetyl acetone	Distilled H_2O	Acetic acid
Titanium sol	22.93g	8.11g	200ml	4.82g

Table 3: Percentage Degradation Efficiency of Pure and Ag doped TiO_2.

Time	A_o	A_t	% Degradation
30 minutes (Pure TiO_2)	1.4273	0.7646	46 %
30 minutes (Ag-TiO_2)	1.4273	0.6653	53 %
45 minutes (Pure TiO_2)	1.4273	0.5655	61 %
45 minutes (Ag-TiO2)	1.4273	0.457	68 %
60 minutes (Pure TiO_2)	1.4273	0.379	73 %
60 minutes (Ag-TiO2)	1.4247	0.2538	82 %

Comparison of photodegradation performance for Pure TiO_2 and Ag–TiO_2 under UV irradiation.

Table 4: XRD Spectra.

2θ	FWHM (°)	FWHM Radian	Crystallite Size (nm)	d-spacing	Planes (hkl)
25.3193	0.2928	0.00511	29.10	3.52149	(101)
36.9582	0.3119	0.00544	28.11	2.43337	(103)
37.7891	0.3135	0.00547	28.03	2.37986	(004)
38.5870	0.3152	0.0055	26.12	2.33482	(112)
48.0727	0.3373	0.00588	26.99	1.89350	(200)
51.9932	0.307	0.002129	25.73	1.70114	(202)
53.8894	0.3535	0.006169	26.38	1.66720	(105)
55.1013	0.3572	0.0062343	26.18	1.49402	(211)
62.1433	0.3805	0.0066409	25.51	1.48107	(213)
62.7123	0.3825	0.006673	23.46	1.3690	(204)
68.7844	0.4057	0.0070808	24.83	1.3360	(116)
70.3438	0.4123	0.007195	24.61	1.3709	(220)

XRD results confirm the crystalline nature of TiO_2 with predominant anatase phase reflections corresponding to the (101), (004), and (200) planes.

Table 5: EDX Analysis.

Element	Line Type	Apparent Concentration	k Ratio	Wt%	Wt% Sigma	Standard Label
O	K series	16.29	0.05483	42.37	1.08	SiO2
Ti	K series	41.73	0.4173	56.57	1.08	Ti
Ag	L series	0.76	0.00756	1.06	0.36	Ag
Total:				100		

The EDX spectrum confirms the presence of Ti, O, and Ag elements, validating the successful doping of Ag into the TiO_2 matrix.

25–27 nm were dispersed. The addition of polyethylene glycol (PEG) during synthesis likely influenced particle growth, reducing TiO_2 crystallite size and modifying morphology.

The smaller $AgNO_3$ nanoparticles are expected to act as electron sinks, reducing recombination and enabling more effective charge separation. This structural modification is consistent with the observed improvement in photocatalytic activity of doped catalysts as show in Figure 14.

Energy Dispersive X-ray Spectroscopy (EDS)

The elemental composition of the synthesized Ag–TiO_2 nanoparticles was confirmed by Energy Dispersive X-ray Spectroscopy (EDS), as shown in Figure 15. The spectrum exhibits distinct peaks corresponding to titanium (Ti), oxygen (O), and silver (Ag), verifying the successful formation of Ag-doped TiO_2 nanostructures.

The strong peaks of Ti and O indicate the presence of TiO_2 as the main constituent of the sample. The high-intensity Ti peak near 4.5–4.8 keV and the O peak at approximately 0.5 keV are characteristic signals of TiO_2. In addition, the presence of a weaker but well-defined Ag peak around 3 keV confirms the successful incorporation of silver into the TiO_2 matrix as shown in Figure 15.

The absence of additional impurity peaks in the spectrum demonstrates the high purity of the synthesized material. These results, in combination with XRD and FTIR analyses, further confirm that Ag is effectively doped into the TiO_2 lattice without the formation of secondary phases. The incorporation of Ag is expected to enhance the photocatalytic performance of TiO_2 by improving charge separation efficiency and reducing electron–hole recombination (Figure 15) and EDX Analysis as shown in Table 5.

Discussion

The combined photocatalytic and characterization results clearly demonstrate that $AgNO_3$ doping significantly enhances the performance of TiO_2 for methylene blue (MB) degradation. This improvement can be attributed to multiple synergistic factors. First, silver nanoparticles act as electron traps, which suppress recombination and extend the lifetime of photogenerated carriers, thereby facilitating more efficient redox reactions. Second, FTIR analysis revealed an increase in surface hydroxyl groups upon doping, promoting the generation of hydroxyl radicals (·OH), which are key oxidizing species in the degradation process. Third, SEM observations showed that PEG-assisted synthesis and $AgNO_3$ incorporation led to reduced TiO_2 particle size and modified surface morphology, providing a greater number of active sites for photocatalysis. In addition, XRD analysis suggested that silver addition helps stabilize the anatase phase, which is known to exhibit higher photocatalytic activity than rutile. Finally, environmental factors such as pH, dye concentration, and irradiation time were found to strongly influence efficiency, with alkaline conditions and longer exposure times favoring higher degradation rates. Collectively, these findings confirm that $AgNO_3$–TiO_2 nanocomposites outperform pure TiO_2 in degrading organic pollutants such as methylene blue and highlight important design parameters for developing effective photocatalysts for wastewater treatment applications.

References

1. Fujishima, Akira, and Kenichi Honda. “Electrochemical photolysis of water at a semiconductor electrode.” *nature* 238.5358 (1972): 37-38.
2. Finegold, Leonard, and Jesse L. Cude. “Biological sciences: One and two-dimensional structure of alpha-helix and beta-sheet forms of poly (L-Alanine) shown by specific heat measurements at low temperatures (1.5–20 K).” *Nature* 238.5358 (1972): 38-40.
3. Anpo, Masakazu, and Masato Takeuchi. “The design and development of highly reactive titanium oxide photocatalysts operating under visible light irradiation.” *Journal of catalysis* 216.1-2 (2003): 505-516.
4. Chen, X. 2009. Titanium dioxide nanomaterials and their energy applications. *Cuihua Xuebao / Chinese J. Catal.* 30:839–851.
5. Anpo, Masakazu, and Masato Takeuchi. “The design and development of highly reactive titanium oxide photocatalysts operating under visible light irradiation.” *Journal of catalysis* 216.1-2 (2003): 505-516.
6. Nolan, N. 2010. Sol-Gel Synthesis and Characterisation of Novel Metal Oxide Nanomaterials for Photocatalytic Applications. *Doctoral* 4032.
7. Sayilkan, F., M. Asiltürk, H. Sayilkan, Y. Önal, M. Akarsu and E. Arpaç. 2005. Characterization of TiO_2 synthesized in alcohol by a sol-gel process: The effects of annealing temperature and acid catalyst. *Turkish J. Chem.* 29:697–706.

8. Hanaor, D. A. H., Gerry Triani, and Charles C. Sorrell. "Morphology and photocatalytic activity of highly oriented mixed phase titanium dioxide thin films." *Surface and coatings technology* 205.12 (2011): 3658-3664.

9. Moon, Eun-Yi, et al. "An increase in mouse tumor growth by an in vivo immunomodulating effect of titanium dioxide nanoparticles." *Journal of Immunotoxicology* 8.1 (2011): 56-67.

10. Gupta, Shipra Mital, and Manoj Tripathi. "A review of TiO2 nanoparticles." *Chinese science bulletin* 56.16 (2011): 1639-1657.

11. Sun, Jirun, et al. "Improving performance of dental resins by adding titanium dioxide nanoparticles." *Dental Materials* 27.10 (2011): 972-982.

12. Ahmed, Ra'ouf, and Haya Abdel. "Preparation and Characterization of Copper-Doped and Silver-Doped Titanium Dioxide Nano-Catalysts for Photocatalytic Applications." (2015).

13. Mahmoodi, Niyaz Mohammad. "Binary catalyst system dye degradation using photocatalysis." *Fibers and Polymers* 15.2 (2014): 273-280.

14. Tan, S.S., L. Zou and E. Hu. 2006. Photocatalytic reduction of carbon dioxide into gaseous hydrocarbon using TiO2 pellets. *Catal. Today* 115:269–273.

15. Erdogan, D.A., M. Polat, R. Garifullin, M.O. Guler and E. Ozensoy. 2014. Thermal evolution of structure and photocatalytic activity in polymer microsphere templated TiO_2 microbowls. *Appl. Surf. Sci.* 308:50–57.

16. Hussain, M., R. Ceccarelli, D.L. Marchisio, D. Fino, N. Russo and F. Geobaldo. 2010. Synthesis, characterization, and photocatalytic application of novel TiO_2 nanoparticles. *Chem. Eng. J.* 157:45–51.

17. Kavitha et al., 2013Ishibai, Y., J. Sato, T. Nishikawa and S. Miyagishi. 2008. Synthesis of visible-light active TiO_2 photocatalyst with Pt-modification: Role of TiO_2 substrate for high photocatalytic activity. *Appl. Catal. B Environ.* 79:117–121.

18. Kavitha et al., 2013Ishibai, Y., J. Sato, T. Nishikawa and S. Miyagishi. 2008. Synthesis of visible-light active TiO_2 photocatalyst with Pt-modification: Role of TiO_2 substrate for high photocatalytic activity. *Appl. Catal. B Environ.* 79:117–121.

19. Hussain, M., R. Ceccarelli, D.L. Marchisio, D. Fino, N. Russo and F. Geobaldo. 2010. Synthesis, characterization, and photocatalytic application of novel TiO_2 nanoparticles. *Chem. Eng. J.* 157:45–51.

20. Chen, X. 2009. Titanium dioxide nanomaterials and their energy applications. *Cuihua Xuebao / Chinese J. Catal.* 30:839–851

21. Sohrabi, M.R. and M. Ghavami. 2008. Photocatalytic degradation of Direct Red 23 dye using UV-TiO_2: Effect of operational parameters. *J. Hazard. Mater.* 153:1235–1239

22. X. Wei, et al., Synthesis, characterization, and photocatalysis of well-dispersible phase-pure anatase TiO2 nanoparticles, Int. J. Photoenergy 2013 (2013).